NANO LETTERS

2007
Vol. 7, No. 5
1308−1313

# Solution–Liquid–Solid (SLS) Growth of ZnSe–ZnTe Quantum Wires having Axial Heterojunctions

**Angang Dong,[†,§] Fudong Wang,[†,§] Tyrone L. Daulton,[‡,§] and William E. Buhro*[,†,§]**

*Departments of Chemistry and Physics and Center for Materials Innovation, Washington University, St. Louis, Missouri 63130-4899*

*Received February 5, 2007; Revised Manuscript Received March 18, 2007*

**ABSTRACT**

**Heterostructured ZnSe–ZnTe quantum wires are grown by the solution–liquid–solid (SLS) mechanism. The nature of the axial or radial heterostructure obtained is strongly influenced by the growth sequence and related synthetic conditions. Compositionally graded $ZnSe_xTe_{1-x}$ wires, ZnSe–ZnTe axial heterostructures containing a $ZnSe_xTe_{1-x}$ transitional segment, ZnSe–ZnTe wires with sharp axial heterojunctions, and radial core–shell ZnSe–ZnTe quantum wires have been selectively prepared. The axial and radial quantum-wire heterostructures are characterized microscopically and spectroscopically.**

We report heterojunction formation in ZnSe−ZnTe quantum wires grown by the solution−liquid−solid mechanism. Both axial (longitudinal) and radial heterostructures were formed, depending on the synthetic pathway followed. The nature of the heterostructures was determined microscopically and spectroscopically.

The great interest in nanostructured materials with tunable sizes, compositions, and morphologies has stimulated efforts to control crystallization at microscopic levels.[1] Recent advances in the preparation of high-quality semiconductor nanostructures, including quantum dots,[2−4] rods,[5,6] and wires,[7−10] have established a wealth of knowledge about their size- and shape-dependent properties. These nanostructures are also the key building blocks for the "bottom-up" construction of nanoscale devices.[11−14]

Fabrication of nanostructures with greater complexity, which will introduce many new opportunities for enhancing the functionality, has become increasingly important to the development of nanoelectronic and nanophotonic systems.[4,6,12−22] One-dimensional (1D) nanowires with either radially modulated compositions (core−shell heterostructures)[12,13] or axially modulated compositions (longitudinal heterojunctions)[14−19] have been synthesized by *vapor-phase* approaches and have already been utilized to construct various nanodevices. On the other hand, colloidal nanocrystal heterostructures, including core−shell nanoparticles,[4] dot−rod and rod−rod (or tetrapod) heterojunctions,[6,20−22] have also been synthesized through *solution-based* methods. Such colloidal heterostructured nanocrystals can serve as ideal models for investigating the intrinsic physics of, for example, carrier separation in complex nanostructures, as they often exhibit dramatic changes in their absorption and/or emission spectra compared with those of single-component nanocrystals.[6,22]

Among the heterostructures currently available, semiconductor *nanowires* possessing heterojunctions are of particular interest, as they group segments with different functionalities in the same wire and are expected to exhibit unique photonic and electrical properties.[14−19] For example, a single semiconductor nanowire containing a p-type segment and an n-type segment can be used as an intrawire p−n junction, which has found applications in field-effect transistors (FETs) and single-nanowire light-emitting diodes (LEDs).[14] Current strategies to combine different segments in a single wire rely mainly on the vapor−liquid−solid (VLS) mechanism in which the alternate growth of different segments can be relatively easily achieved by repeated modulation of the vapor-phase reactants during growth of the wires. To date, GaP−GaAs,[14,18] Si−SiGe,[15] InP−InAs,[16] and (p-type) InP−(n-type) InP[14] nanowire heterojunctions have been synthesized by this mechanism.

As an analogy to the traditional VLS mechanism, the solution−liquid−solid (SLS) growth process has proven to be an alternative general mechanism to synthesize high-quality semiconductor nanowires.[9] In comparison to the VLS mechanism, SLS growth produces nanowires with generally smaller diameters (≤10 nm) within the quantum-confined regime and, in some cases, narrower diameter distributions (std deviation 10−20% of the mean diameter), due to the

* Corresponding author. E-mail: buhro@wustl.edu.
† Department of Chemistry, Washington University.
‡ Department of Physics, Washington University.
§ Center for Materials Innovation, Washington University.

10.1021/nl070293v CCC: $37.00 
**Published on Web 03/28/2007**

lower synthesis temperatures (180−300 °C) employed in solution. Furthermore, the as-synthesized nanowires are soluble (dispersible) in conventional solvents, assisting spectroscopic studies and efforts to control nanowire surface functionalization. The SLS method has been successfully employed to prepare semiconductor nanowires with a wide range of compositions.[9]

We chose ZnSe−ZnTe as an initial system to study intrawire heterojunction formation because ZnTe and ZnSe nanowires may be prepared under similar SLS-growth conditions. Moreover, ZnTe and ZnSe are easily doped p-type and n-type, respectively,[23] which should further assist carrier separation in ZnTe−ZnSe intrawire p−n junctions. To our knowledge, this is the second report of the fabrication of semiconductor nanowire heterojunctions through a solution-based approach.

The first such report was by Park and co-workers,[24] in which heterostructured CdS−CdSe nanowires were grown by the SLS mechanism from Bi particles anchored to a support. Sharp axial (longitudinal) heterojunctions were formed, as demonstrated by transmission-electron-microscopy (TEM) images and energy-dispersive X-ray spectroscopy (EDS). However, the diameters of the CdSe (20−130 nm) and CdS (15−80 nm) segments were fairly large and outside the quantum-confinement regime. In our study, the heterostructured nanowire diameters were generally much smaller (7−12 nm), and so the nanowires are true quantum wires. Consequently, heterostructure formation here is additionally verified by absorption spectroscopy, confirming the quantum confinement in the differing segments of the nanowires. The following sections describe the formation of quantum wires in the Zn−Se−Te system under varying conditions, affording compositionally graded $ZnSe_xTe_{1-x}$ wires, ZnSe−ZnTe axial heterostructures containing a $ZnSe_xTe_{1-x}$ transitional segment, ZnSe−ZnTe wires with sharp axial heterojunctions, and core−shell ZnSe−ZnTe quantum wires. Detailed synthetic procedures are provided in the Supporting Information.

**Binary ZnTe and ZnSe Quantum Wires.** To support studies of heterostructure formation, the independent synthesis of ZnTe and ZnSe nanowires was pursued first. Fortunately, these nanowires were successfully grown by the SLS mechanism under similar conditions, including a common 1-octadecene (ODE) solvent, a common zinc-stearate precursor ($Zn(SA)_2$), a common Bi-nanoparticle catalyst (diameters = 8−16 nm),[9e] similar surface-capping ligands including tri-*n*-octylphosphine oxide (TOPO), tri-*n*-octylphosphine (TOP), and 1-hexadecylamine (HDA), and similar growth temperatures in the range of 290−310 °C (see the Supporting Information).

The optimal synthesis of ZnTe nanowires required the $Zn(SA)_2$ and tri-*n*-butylphosphine telluride (TBPTe) precursors in molar ratios of 8:1−9:1, whereas the optimal synthesis of ZnSe nanowires required the $Zn(SA)_2$ and tri-*n*-octylphosphine selenide (TOPSe) precursors in approximately the *reverse* molar ratios of 1:6−1:10. The resulting wire diameters were largely determined by the diameters of the Bi nanoparticles and were purposefully varied in the range of 6−14 nm.

Both the ZnTe and ZnSe nanowires exhibited quantum-confinement effects in their absorption spectra due to their small diameters. For example, ZnTe (∼10 nm in diameter) and ZnSe nanowires (∼12 nm in diameter) showed first-excitonic transitions at ∼520 and ∼450 nm, respectively, which were blue-shifted with respect to the bulk band gap energies (Figure S1, Supporting Information). Both the ZnTe and ZnSe quantum wires were single crystalline, as confirmed by selected-area electron diffraction (SAED) patterns (Figure S2, Supporting Information) and high-resolution TEM (HRTEM) images (Figure S3, Supporting Information).

**Alloyed Ternary $ZnSe_xTe_{1-x}$ Nanowires Having a Compositional Gradient.** In an initial attempt to prepare ZnSe−ZnTe nanowire heterostructures, a solvent dispersion of $Zn(SA)_2$, TBPTe, surface-capping ligands, and Bi-catalyst nanoparticles was heated at 290 °C. The reaction was allowed to proceed for about 2 min, when the solution color turned to orange, indicating the growth of ZnTe−nanowire segments. The reaction vessel was then transferred to 300 °C, and TOPSe was quickly injected to promote the subsequent growth of ZnSe nanowire segments on the initially grown ZnTe segments. The quantity of Bi nanoparticles employed was minimized to prevent the formation of separate ZnSe nanowires.

However, subsequent analysis established that most of the nanowires generated by this procedure consisted of $ZnSe_xTe_{1-x}$ alloys with a composition gradient along the wire axis. Figure 1a gives a typical TEM image of such nanowires, with an average diameter of 10 nm. The chemical composition of the selected wire was determined by EDS, which gave Se:Te elemental ratios from spot 1 to spot 4 of 3.9:1, 2.7:1, 1.4:1, and 1.0:1, respectively. The gradual decrease of the Se:Te ratio from the Bi tip (Figure 1a inset) to the opposite end reveals a composition gradient along the wire growth axis.

The overall crystallinity of the nanowire ensemble was examined by powder X-ray diffraction (XRD). A single set of diffraction peaks, each located between the corresponding positions of the lines in the bulk hexagonal ZnTe and ZnSe phases, was observed (Figure S4, Supporting Information), confirming the alloyed crystal structures of the wires. The peaks were significantly broadened by the gradient nature of the wires.

Although both ZnTe and ZnSe nanowires show a resolvable excitonic feature in their absorption spectra (Figure S1), no discernible features were found in the spectra of the alloyed wires (Figure 1b), further confirming the gradient nature of the alloyed wires. The absence of an excitonic feature around 450 nm arising from ZnSe implied that the growth of independent ZnSe nanowires from free Bi nanoparticles was limited. Taken together, the chemical and structural data showed that nanowires grown by this approach were alloyed wires without apparent heterojunctions.

We surmised that only short ZnTe wire or rod segments were generated during the initial 2 min reaction period, such that a considerable amount of Zn and Te precursors remained

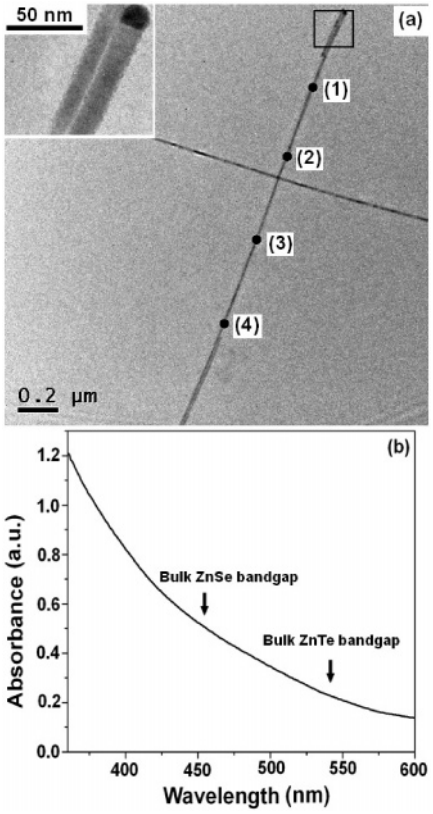


**Figure 1.** (a) TEM image of ternary $ZnSe_xTe_{1-x}$ nanowires. The inset shows a higher-magnification TEM image of the selected area highlighted by the square. The black dots on the wire show the spots where EDS spectra were collected (see text). (b) Absorption spectrum of the sample. The arrows indicate the bulk band gap energies of ZnSe and ZnTe, respectively.

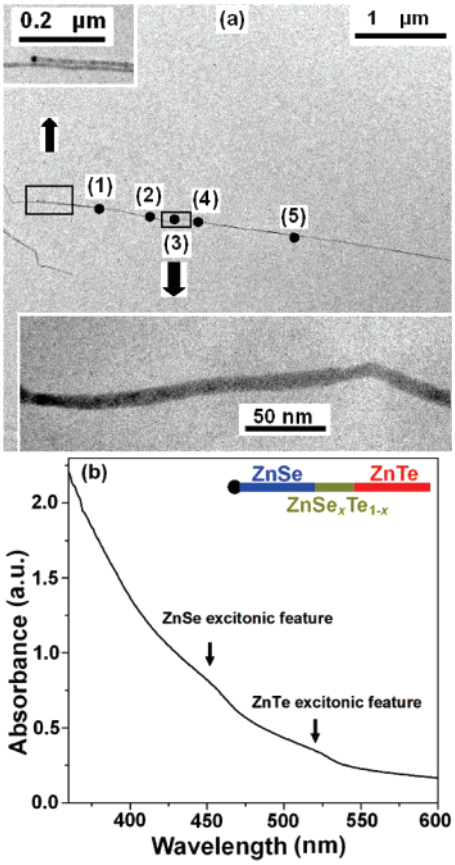


**Figure 2.** (a) TEM image of a representative ZnSe−ZnTe nanowire with a three-segment heterojunction structure. The insets show higher-magnification TEM images of the selected areas highlighted by the rectangles. The black dots on the wire represent the spots where EDS spectra were collected (see text). (b) Absorption spectrum of the sample. The arrows indicate the first-excitonic transitions arising from the ZnSe and ZnTe segments, respectively. The inset shows a cartoon depicting the three-segment heterojunction structure.

unreacted. After the introduction of TOPSe, Se and Te precursors co-reacted to produce the ternary, alloyed wires. With the continued growth of the wires and the consumption of Te species, the Se:Te ratio gradually increased, resulting in the observed compositional gradient along the wire growth axis. No excitonic features attributed to the pure ZnTe portions could be observed in the absorption spectra, presumably due to their short lengths and thus small quantities compared to the gradient wire segments.

**ZnSe−ZnTe Nanowire Heterostructures Containing a $ZnSe_xTe_{1-x}$ Segment.** In a second attempt to generate sharp ZnSe−ZnTe heterojunctions, the conditions were modified to increase consumption of the Te precursor before attempted growth of the subsequent ZnSe nanowire segments. Thus additional $Zn(SA)_2$ was added after the initial 2 min reaction period, and the reaction was allowed to proceed for another 1 min before the injection of TOPSe. By this approach, nanowires with a three-segment heterostructure were obtained.

A TEM image of a representative nanowire grown by this approach is shown in Figure 2a (diameter ≈ 10 nm). EDS spectra (Figure S5, Supporting Information) collected from selected spots along the wire axis showed that the segment attached to the Bi tip (Figure 2a, upper-left inset) was composed of ZnSe, while the opposite side of the wire was composed of ZnTe. A segment with a length of ca. 200 nm (Figure 2a, bottom inset) embedded between the ZnSe and ZnTe segments was found to contain Zn, Se, and Te, consistent with a ternary $ZnSe_xTe_{1-x}$ transitional region between the ZnTe to ZnSe segments. A cartoon depicting this wire heterostructure is given in the inset of Figure 2b. All five nanowires examined from this sample exhibited a similar three-segment heterostructure with a ternary $ZnSe_xTe_{1-x}$ transition section sandwiched between ZnSe and ZnTe segments.

Two resolvable excitonic transitions, arising from ZnSe segments ($\lambda \sim 450$ nm) and ZnTe segments ($\lambda \sim 520$ nm), respectively, were found in the absorption spectrum (Figure 2b) of these three-segment nanowires. As expected, the $ZnSe_xTe_{1-x}$ transition section did not exhibit a discernible excitonic feature. Both ZnTe and ZnSe crystal phases were observed in the XRD pattern (Figure S6, Supporting Information). The formation of the ternary transitional segment in these nanowire heterostructures indicated that unreacted Te precursor remained when TOPSe was introduced, although the amount was greatly reduced by the subsequent aliquot of $Zn(SA)_2$.

**ZnSe−ZnTe Nanowire Heterostructures with Sharp Axial Interfaces.** We recognized the desirability of the

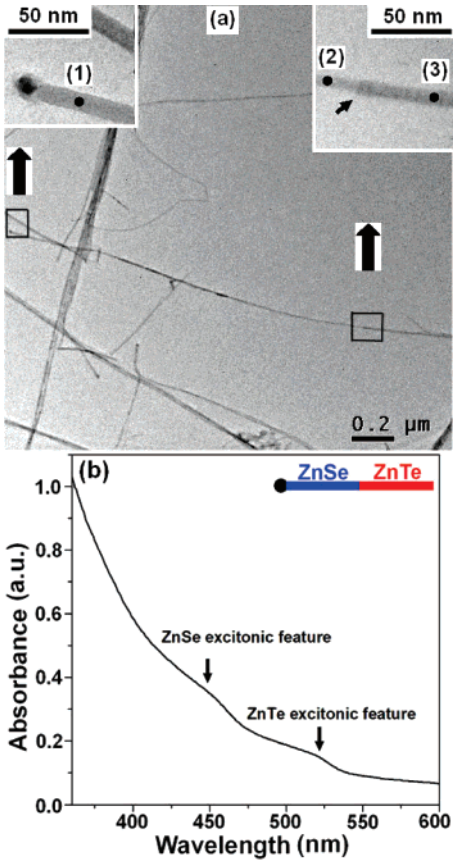


**Figure 3.** (a) TEM image of a representative ZnSe−ZnTe nanowire heterojunction with a sharp interface. The insets show higher-magnification TEM images of the sections highlighted by the squares, and the black dots indicate the spots where EDS spectra were collected (see text). The arrow in the upper-right inset shows the interface between the two wire segments. (b) Absorption spectrum from the sample shown in (a). The arrows indicate the first-excitonic features arising from ZnSe and ZnTe segments, respectively.

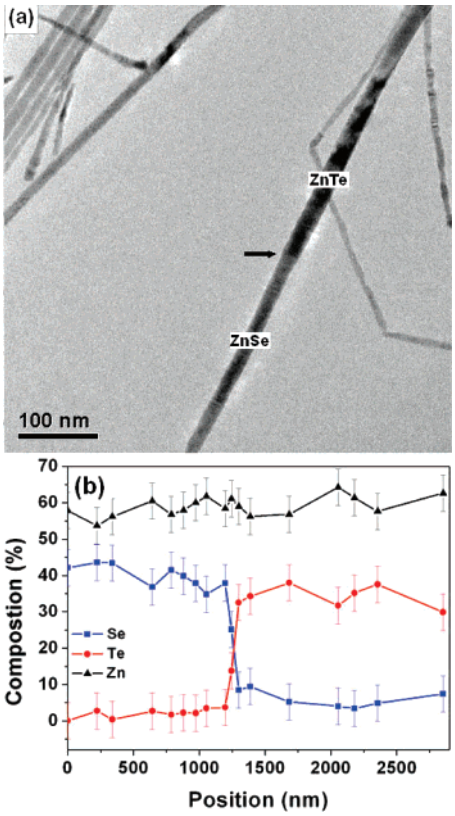


**Figure 4.** (a) TEM image of a second ZnSe−ZnTe nanowire heterojunction with a sharp interface (indicated by an arrow), showing that the ZnTe segment is slightly thicker than the ZnSe segment. (b) EDS line profiles of the same wire as shown in (a), showing the change of composition as function of position. The slightly higher Zn signal relative to the Se and Te signals may be due to the partial overlap of an adjacent Cu EDS peak from the TEM grid with the Zn peak. The apparent remnant Se signal in the right section could be caused by Se attachment onto the preformed ZnTe-wire surface.

complete removal of unreacted Te species to achieve sharp ZnSe−ZnTe nanowire heterojunctions. This goal was achieved by isolation and purification of the as-synthesized ZnTe nanowires prior to growth of the ZnSe segments. Precipitated ZnTe nanowires were redispersed in a TOPSe solution and then quickly injected into a reaction mixture containing Zn-$(SA)_2$ and ligands at 300 °C to afford ZnSe−ZnTe nanowire heterojunctions with sharp interfaces. Air exposure of the isolated ZnTe wires was kept brief (<2 min) to prevent decomposition of the ZnTe wires and to retain the catalytic activity of the Bi tips.

A TEM image of nanowires with a mean diameter = 11 nm synthesized by this approach is shown in Figure 3a. EDS analyses of the wire segment attached to the Bi tip (Figure 3a, upper-left inset) and of the opposite end of the wire confirmed the ZnSe and ZnTe compositions, respectively (Figure S7, Supporting Information). An EDS analysis (spot size ≈ 100 nm) taken at the interface indicated the presence of both ZnSe and ZnTe, as expected. Because of the higher *Z* of Te, the ZnTe segment appears darker in the TEM image, such that the interface between two segments could be identified (Figure 3a, upper-right inset).

A TEM image of a thicker ZnSe−ZnTe nanowire heterojunction (~22 nm in diameter) is shown in Figure 4a, and the EDS line scan along the wire at lower magnification (Figure S8, Supporting Information) confirmed the composition variation across the interface (Figure 4b).

A representative HRTEM image of the junction region in another wire (~12 nm in diameter) is shown in Figure 5. The clear lattice fringes suggest the epitaxial relationship of the two wire segments and the wire's high crystallinity. In addition to the different lattice fringe spacings between two wire segments, the Fourier transform from the high-resolution image containing the junction region showed the splitting of the diffraction peaks (Figure 5, middle inset), further confirming the existence of an interface between two wire segments. The thickness of the transition region between the two segments appeared to be ≤6 nm.

We observed that, in many cases, the ZnTe segment was slightly thicker (by 1−2 nm) than the ZnSe segment at the interface (Figures 3a, 4a, and 5). We surmised that this might have been due to slightly different contact angles formed by the bismuth catalyst droplets with the ZnSe and ZnTe surfaces. Similar results were also found by Park and co-workers in the preparation of CdS−CdSe nanowire hetero-

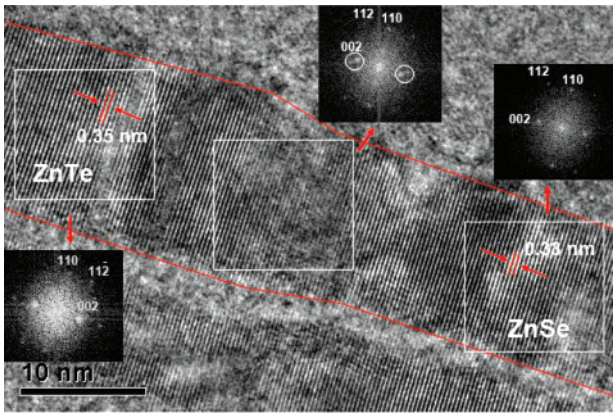


**Figure 5.** HRTEM image of another single ZnSe−ZnTe wire with a sharp interface, showing growth along the [002] lattice direction in the [2$\bar{2}$0] zone axis and confirming the epitaxial relationship of the two wire segments and the wire's high crystallinity. The [002] lattice-fringe spacings (0.35 nm for ZnTe segment and 0.33 nm for ZnSe segment) are consistent with the standard values. The insets show the Fourier transforms calculated from the high-resolution images (indicated by squares) of the ZnTe-segment region, the junction region, and the ZnSe-segment region, respectively. The middle Fourier transform from the image containing the junction region shows a splitting of the diffraction peaks along the [002] lattice direction.

junctions.[24] The majority of wires examined were heterostructured, although some binary ZnTe and ZnSe wires were also found, presumably resulting from deactivated Bi tips and free Bi nanoparticles, respectively.

As for the three-segment heterostructures above, the absorption spectra of the ZnSe−ZnTe heterojunction nanowires obtained by this approach exhibited two resolvable excitonic features, which were assigned to the ZnSe ($\lambda \sim$ 450 nm) and ZnTe ($\lambda \sim$ 520 nm) segments, respectively (Figure 3b). Both the ZnTe and ZnSe crystal phases were observed in the XRD pattern (Figure S9, Supporting Information). The 110 reflections of the ZnTe and ZnSe phases were unshifted from the standard values, precluding the presence of significant amounts of crystalline $ZnSe_xTe_{1-x}$ alloy in the wires.

**Core−Shell ZnSe−ZnTe Nanowires Obtained by Reversing the Growth Sequence.** Each of the above approaches proceeded by deposition of ZnSe onto preformed ZnTe wires. The reversed sequence, in which ZnTe was deposited onto preformed ZnSe wires under conditions similar to those used above, failed to produce nanowire heterojunctions. Rather, ZnSe−ZnTe core−shell nanowires were obtained.

The TEM image in Figure 6a revealed the core−shell heterostructures of these nanowires. Analyses by EDS and XRD confirmed that the irregular shells were composed of amorphous or poorly crystalline ZnTe. Subtle changes in the absorption spectrum of the ZnSe nanowires were observed upon shell formation (Figure 6b). In the absorption spectrum of the core−shell nanowires, the first excitonic feature corresponding to ZnSe ($\lambda \sim$ 450 nm) was essentially unshifted, but weakened in comparison to the second excitonic feature ($\lambda \sim$ 390 nm). No feature was observed for the ZnTe shell. Interestingly, the second ZnSe excitonic

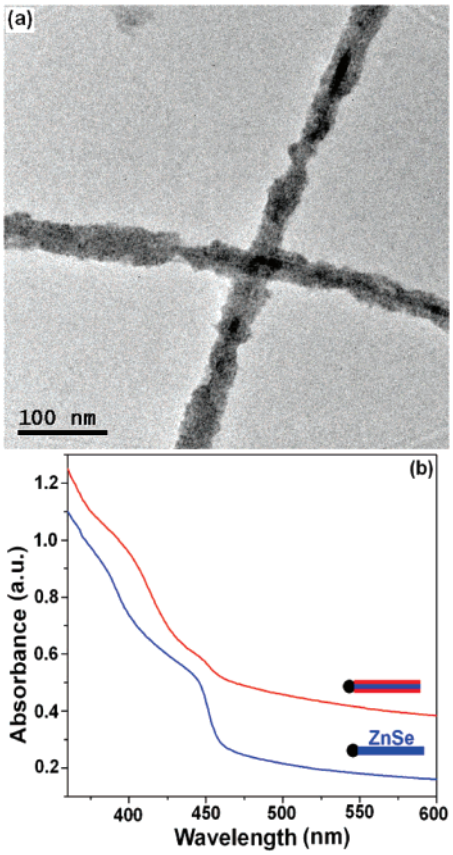


**Figure 6.** (a) TEM image of ZnSe−ZnTe core−shell nanowire heterostructures. (b) Absorption spectra of the same ZnSe−ZnTe core−shell sample (red curve) and the ZnSe core nanowires (blue curve) used in its preparation.

feature appeared to be red-shifted. The lack of a shift in the first excitonic feature suggests that the shell induced only a minor perturbation on the electronic structure of the ZnSe quantum wires.

The results established that the growth sequence had a profound effect on the resulting core−shell vs axial−heterojunction structure. A related phenomenon was observed by Alivisatos and co-workers in the preparation of colloidal semiconductor nanorod or tetrapod heterostructures.[6] In that work, the growth sequence was also found to determine whether core−shell or axial−heterojunction architectures were produced. The formation of the core−shell structure here also implies that ZnTe−ZnSe nanowires with multiple axial heterojunctions cannot be produced by repeated switching of the Te and Se precursors without a further modification of the procedure.

In conclusion, the work described here and that reported earlier by Park and co-workers[24] establishes that formation of sharp axial heterojunctions should be routinely achievable over large diameter and compositional ranges by the SLS method. The key to formation of sharp axial interfaces is the effective switching between precursors corresponding to the two compositions. Thus, the precursors corresponding to the first composition must be completely consumed or removed prior to introduction of the precursors for the second. This is achieved ingeniously by Park and co-workers by the SLS growth of nanowires anchored to a substrate,

which can be readily switched between the alternate precursor solutions. In this study, such axial heterojunctions are achieved in smaller, quantum-confined wires. Future work is aimed at identifying the factors that distinguish between axial deposition of the second phase to form axial heterojunctions vs surface deposition on the first phase to form core−shell nanowires. Control of this deposition morphology will allow more complex nanowire heterostructures to be grown by the SLS method.

**Acknowledgment.** We thank Professor Richard Loomis and Jianwei Sun for helpful discussions, and the National Science Foundation (grant no. CHE-0518427) for support of this work. A. D. is grateful to the Washington University Graduate School of Arts and Sciences for a one-semester research fellowship.

**Supporting Information Available:** Detailed synthetic procedures, UV−visible absorption spectra, SAED patterns, HRTEM and TEM images, XRD patterns, and EDS spectra. This material is available free of charge via the Internet at http://pubs.acs.org.

## References

(1) (a) Alivisatos, A. P. *Science* **1996**, *271*, 933. (b) Jun, Y.; Choi, J.; Cheon, J. *Angew. Chem., Int. Ed.* **2006**, *45*, 3414. (c) Xia, Y.; Yang, P.; Sun, Y.; Wu, Y.; Mayers, B.; Gates, B.; Yin, Y.; Kim, F.; Yan, H. *Adv. Mater.* **2003**, *15*, 353.
(2) Murray, C. B.; Norris, D. J.; Bawendi, M. G. *J. Am. Chem. Soc.* **1993**, *115*, 8706.
(3) Peng, Z.; Peng, X. *J. Am. Chem. Soc.* **2002**, *124*, 3343.
(4) Battaglia, D.; Blackman, B.; Peng, X. *J. Am. Chem. Soc.* **2005**, *127*, 10889.
(5) Peng, X.; Manna, L.; Yang, W.; Wickham, J.; Scher, E.; Kadavanich, A.; Alivisatos, A. P. *Nature* **2000**, *404*, 59.
(6) Milliron, D. J; Hughes, S. M; Cui, Y.; Manna, L.; Li, J.; Wang, L.; Alivisatos, A. P. *Nature* **2004**, *430*, 190.
(7) Morales, A. M.; Lieber, C. M. *Science* **1998**, *279*, 208.
(8) Duan, X.; Lieber, C. M. *Adv. Mater.* **2000**, *12*, 298.
(9) (a) Wang, F.; Dong, A.; Sun, J.; Tang, R.; Yu, H.; Buhro, W. E. *Inorg. Chem.* **2006**, *45*, 7511. (b) Trentler, T. J.; Hickman, K. M.; Goel, S. C.; Viano, A. M.; Gibbons, P. C.; Buhro, W. E. *Science* **1995**, *270*, 1791. (c) Yu, H.; Li, J.; Loomis, R. A.; Wang, L.; Buhro, W. E. *Nat. Mater.* **2003**, *2*, 517. (d) Yu, H.; Buhro, W. E. *Adv. Mater.* **2003**, *15*, 416. (e) Yu, H.; Li, J.; Loomis, R. A.; Gibbons, P. C.; Wang, L.; Buhro, W. E. *J. Am. Chem. Soc.* **2003**, *125*, 16168. (f) Grebinski, J. W.; Hull, K. L.; Zhang, J.; Kosel, T. H.; Kuno, M. *Chem. Mater.* **2004**, *16*, 5260.
(10) Holmes, J. D.; Johnston, K. P.; Doty, R. C.; Korgel, B. A. *Science* **2000**, *287*, 1471.
(11) Huynh, W. U.; Dittmer, J. J.; Alivisatos, A. P. *Science* **2002**, *295*, 2425.
(12) Lauhon, L. J.; Gudiksen, M. S.; Wang, D.; Lieber, C. M. *Nature* **2002**, *420*, 57.
(13) Li, Y.; Xiang, J.; Qian, F.; Gradecak, S.; Wu, Y.; Yan, H.; Blom, D. A.; Lieber, C. M. *Nano Lett.* **2006**, *6*, 1468.
(14) Gudiksen, M. S.; Lauhon, L. J.; Wang, J.; Smith, D. C.; Lieber, C. M. *Nature* **2002**, *415*, 617.
(15) Wu, Y.; Fan, R.; Yang, P. *Nano Lett.* **2002**, *2*, 83.
(16) Björk, M. T.; Ohlsson, B. J.; Sass, T.; Persson, A. I.; Thelander, C.; Magnusson, M. H.; Deppert, K.; Wallenberg, L. R.; Samuelson, L. *Nano Lett.* **2002**, *2*, 87.
(17) Wu, Y.; Xiang, J.; Yang, C.; Lu, W.; Lieber, C. M. *Nature* **2004**, *420*, 61.
(18) Verheijen, M. A.; Immink, G.; Smet, T. de.; Borgstrom, M. T.; Bakkers, E. P. A. M. *J. Am. Chem. Soc.* **2006**, *128*, 1353.
(19) Yang, C.; Zhong, Z.; Lieber, C. M. *Science* **2005**, *310*, 1304.
(20) Mokari, T.; Rothenberg, E.; Popov, I.; Costi, R.; Banin, U. *Science* **2004**, *304*, 1787.
(21) Kudera, S.; Carbone, L.; Casula, M. F.; Cingolani, R.; Falqui, A.; Snoeck, E.; Parak, W. J.; Manna, L. *Nano Lett.* **2005**, *5*, 445.
(22) (a) Peng, P.; Milliron, D. J.; Hughes, S. M.; Johnson, J. C.; Alivisatos, A. P.; Saykally, R. J. *Nano Lett.* **2005**, *5*, 1809. (b) Halpert, J. E.; Porter, V. J.; Zimmer, J. P.; Bawendi, M. G. *J. Am. Chem. Soc.* **2006**, *128*, 12590.
(23) Lin, W.; Yang, B. X.; Guo, S. P.; Elmoumni, A.; Fernandez, F.; Tamargo, M. C. *Appl. Phys. Lett.* **1999**, *75*, 2608.
(24) Ouyang, L.; Maher, K. N.; Yu, C. L.; McCarty, J.; Park, H. *J. Am. Chem. Soc.* **2007**, *129*, 133.

NL070293V